Author(s): Thirumoorthi, Ramalingam; Chivers, Tristram; Häggman, Susanna; Mansikkamäki, Akseli; Morgan, Ian; Tuononen, Heikki; Lahtinen, Manu; Konu, Jari

Title: Synthesis of a labile sulfur-centred ligand, [S(H)C(PPh2S)2]-: structural diversity in lithium(i), zinc(ii) and nickel(ii) complexes

Year: 2016

Version:

Please cite the original version:

Thirumoorthi, R., Chivers, T., Häggman, S., Mansikkamäki, A., Morgan, I., Tuononen, H., Lahtinen, M., & Konu, J. (2016). Synthesis of a labile sulfur-centred ligand, [S(H)C(PPh2S)2]-: structural diversity in lithium(i), zinc(ii) and nickel(ii) complexes. Dalton Transactions, 45(32), 12691-12701. https://doi.org/10.1039/c6dt02565j

Synthesis of a Labile Sulfur-Centred Ligand, $[S(H)C(PPh_2S)_2]^-$: Structural Diversity in Lithium(I), Zinc(II) and Nickel(II) Complexes†

Ramalingam Thirumoorthi,[a] Tristram Chivers,[a] Susanna Häggman,[b] Akseli Mansikkamäki,[b] Ian S. Morgan,[b] Heikki M. Tuononen,[b] Manu Lahtinen[b] and Jari Konu*[b]

[a] Department of Chemistry, University of Calgary, Calgary, AB T2N 1N4, Canada.

[b] Department of Chemistry, University of Jyväskylä, P.O. Box 35, Jyväskylä, FI-40014, Finland.

* *E-mail*: jari.a.konu@jyu.fi, *Tel.* +358-40-805-4406, *Fax.* +358-14-260-2501

Abstract: A high-yield synthesis of $[Li\{S(H)C(PPh_2S)_2\}]_2$ $[Li_2{\cdot}(\mathbf{3})_2]$ was developed and this reagent was used in metathesis with $ZnCl_2$ and $NiCl_2$ to produce homoleptic complexes **4** and **5b** in 85 and 93 % yields, respectively. The solid-state structure of the octahedral complex $[Zn\{S(H)C(PPh_2S)_2\}_2]$ (**4**) reveals notable inequivalence between the Zn–S(C) and Zn–S(P) contacts (2.274(1) Å vs. 2.842(1) and 2.884(1) Å, respectively). Two structural isomers of the homoleptic complex $[Ni\{S(H)C(PPh_2S)_2\}_2]$ were isolated after prolonged crystallization processes. The octahedral green Ni(II) isomer **5a** exhibits the two monoprotonated ligands bonded in a tridentate (S,S′,S″) mode to the Ni(II) centre with *three* distinctly different Ni–S bond lengths (2.3487(8), 2.4500(9) and 2.5953(10) Å). By contrast, in the red-brown square-planar complex **5b** the two ligands are S,S′-chelated to Ni(II) (*d*(Ni–S) = 2.165(2) and 2.195(2) Å) with one pendant PPh_2S group. DFT calculations revealed that the energetic difference between singlet and triplet state octahedral and square-planar isomers of the Ni(II) complex is essentially indistinguishable. Consistently, VT and ^{31}P CP/MAS NMR spectroscopic investigations indicated that a mixture of isomers exists in solution at room temperature, while the singlet state square-planar isomer **5b** becomes favoured at -40 ^{o}C.

Keywords: nickel · zinc · sulfur ligands · isomerization · electronic structures

Introduction

A synthetic route to the intriguing dithiodiphosphinato-methanediide dianion, $[C(PPh_2S)_2]^{2-}$, was reported by Le Floch and co-workers in 2004 paving the way for the synthesis of metal complexes via metathesis.[1] Early transition-metal complexes can also be used in a transmetalation process to transfer the carbene ligand to late transition metals,[2] and, consequently, a wide variety of transition-metal, p-block element, lanthanide and actinide complexes of the dianion have been examined.[3-5] In most cases the dianion behaves as a tridentate ligand, which is S,C,S-coordinated to the metal centre and the primary interest in such complexes has been on the electronic structure and reactivity of the metal-carbon bond, as well as on the dichotomy with respect to their description as either Fischer carbenes or Schrock alkylidines.[3a,6,7]

In 2010 we described the use of Le Floch's dianion for the synthesis of the trichalcogeno-centred PCP-bridged dianions $[(E)C(PPh_2S)_2]^{2-}$ (**1E**; E = S, Se),[8] prompted by the unexpected discovery of the selenium analogue $[(Se)C(PPh_2Se)_2]^{2-}$ (**1Se**) via an unprecedented Se-H^+ exchange at the carbon centre in reactions of the diseleno PCP-bridged monoanion $[HC(PPh_2Se)_2]^-$ with main group and transition metal halides (Hg, Sn, Te).[9] Early investigations of these trichalcogeno-centred PCP-bridged dianions have revealed a versatile coordination and redox behaviour.[10] For example, while the dianionic ligand **1S** displays the expected S,S′,S″-coordination in octahedral In(III), Sn(IV), Pb(II) and Te(IV) complexes,[11,12] the diversity of these trichalcogeno ligands is evident in the group 11 metal compounds. In the mixed valent Au(I)-Au(III) complexes $Au_2{\cdot}(\mathbf{1E})_2$ (E = S, Se) the dianions $(\mathbf{1E})^{2-}$ act as bridging ligands that are E,E′-chelated to the square-planar Au(III) centre and S-monodentate towards the linear Au(I) atom.[12] By contrast, in the reactions with $CuCl_2$ the dianions in $Li_2{\cdot}\mathbf{1E}$ (E = S, Se) operate as reducing agents to give dinuclear Cu(I)-Cu(I) complexes in which the two Cu(I) centres are formally bridged by two radical anions $[EC(PPh_2S)_2]^{\bullet-}$ that are

connected by a long E–E bond to form a dimeric dianion, $[(SPh_2P)_2CEEC(PPh_2S)_2]^{2-}$ (**2E**; E = S, Se).[12]

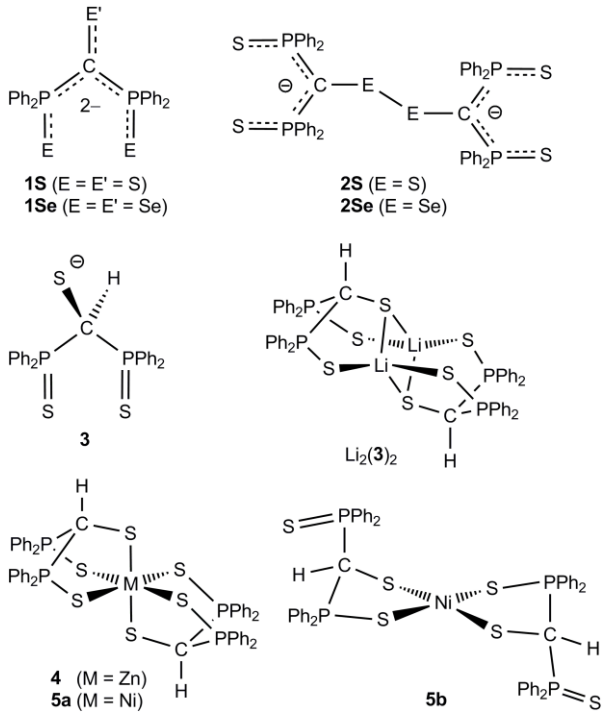

In earlier investigations we noticed the proclivity of the dimeric system **2S** to undergo proton abstraction in the metathetical reaction with $ZnCl_2$, which produces the tridentate monoanion $[S(H)C(PPh_2S)_2]^-$ (**3**) in the octahedral complex $[Zn\{S(H)C(PPh_2S)_2\}_2]$ (**4**).[10] In this context we note that the HOMOs of the monomeric and dimeric dianions **1E** and **2E**, respectively, display a significant contribution from the p-orbitals of the PCP-carbon atom, thereby contributing to the apparent tendency for proton abstraction in common organic solvents.[8, 10] Consistently, during the current study a prolonged crystallization process of the reaction between Li_2·**1S** and $NiCl_2$ afforded green crystals of the octahedral Ni(II) complex $[Ni\{S(H)C(PPh_2S)_2\}_2]$ (**5a**) in which two monoanions $[S(H)C(PPh_2S)_2]^-$ (**3**) are S,S′,S″-coordinated to Ni(II); the yield of **5a** was only 12%, presumably as a result of the monoprotonation of **1S**. Serendipitously, at the same time we also isolated small amounts of the red, square-planar isomer **5b** in which the two $[S(H)C(PPh_2S)_2]^-$ (**3**) ligands are S,S′-chelated to the Ni(II) centre leaving a pendant $Ph_2P{=}S$ group. Although the

conversion of four-coordinate to six-coordinate nickel(II) complexes upon coordination of solvent is well-known,[13] the identification of both four- and six-coordinate isomers *incorporating the same ligand* is, to our knowledge, unprecedented.[14]

We have now developed a high-yield synthesis for $[Li\{S(H)C(PPh_2S)_2\}]_2$ $[Li_2\cdot(\mathbf{3})_2]$ and used it to prepare the homoleptic M(II) complexes $[M\{S(H)C(PPh_2S)_2\}_2]$ (**4**, M = Zn; **5**, M = Ni) in excellent yields. In this contribution we describe (a) the synthesis, NMR characterization and X-ray structure of the new reagent $[Li_2\cdot(\mathbf{3})_2]$, (b) the synthesis and structural characterization of the homoleptic complex $[Zn\{S(H)C(PPh_2S)_2\}_2]$ (**4**), (c) single-crystal structures and DFT calculations of the octahedral (O_h) and square-planar (SP) isomers of $[Ni\{S(H)C(PPh_2S)_2\}_2]$ (**5a**, **5b**), and (d) powder X-ray diffraction, ^{31}P VT and CP/MAS NMR as well as UV-Vis spectroscopic investigations of the nickel(II) complex **5**.

Results and Discussion

Synthesis and structural characterization of $[Li\{S(H)C(PPh_2S)_2\}]_2$ $[Li_2\cdot(3)_2]$. Formation of the Zn(II) complex **4** from the dimeric system **2S** and, especially, the intriguing structural dichotomy of the homoleptic Ni(II) complex **5** together with the potentially versatile coordination behaviour of the novel monoanion **3** provided strong incentives to develop a high-yield synthesis of an alkali-metal derivative of the monoanion. This was achieved via a straightforward two-step process in which the neutral dithio compound $[H_2C(PPh_2S)_2]$ was first monodeprotonated with ^{n}BuLi [15,16] and then treated with one equivalent of elemental sulfur in toluene to afford $Li_2\cdot(\mathbf{3})_2$ as an analytically pure, pale yellow powder with toluene solvate in excellent yield (90 %) (Eq. 1 and 2).

$$[H_2C(PPh_2S)_2] + {}^{n}BuLi \rightarrow [Li\{(H)C(PPh_2S)_2\}] + {}^{n}BuH \quad (1)$$

$$2\ [Li\{(H)C(PPh_2S)_2\}]\ +\ ¼\ S_8\ \rightarrow\ [Li\{S(H)C(PPh_2S)_2\}]_2{\cdot}(C_7H_8) \qquad (2)$$

$$[Li_2{\cdot}(\mathbf{3})_2]{\cdot}(C_7H_8)$$

The ^{7}Li and ^{31}P{^{1}H} NMR spectra of $Li_2{\cdot}(\mathbf{3})_2$ in CD_2Cl_2 display the expected singlets at 1.33 and 53.1 ppm, respectively. In the ^{1}H NMR spectrum a singlet is apparent at 2.33 ppm indicating the presence of toluene solvate (CH_3 group). In addition, a triplet is observed at 5.18 ppm (^{2}J (^{31}P,^{1}H) = 7.5 Hz) arising from coupling of the CH hydrogen atom to two equivalent phosphorus atoms of the P(S)C(H)P unit. The phenyl groups in $Li_2{\cdot}(\mathbf{3})_2$ exhibit multiplets in the range 6.89-8.07 ppm. The approximate intensity ratio of the signals in the ^{1}H NMR spectrum of the dimer is 45 (m,$C_6\mathit{H}_5$): 2 (t,PC(*H*)P: 3 (s, $C\mathit{H}_3C_6H_5$).

In contrast to the composition of the initial powdery product, the crystallization of $Li_2{\cdot}(\mathbf{3})_2$ in CH_2Cl_2 produced colourless crystals without solvent incorporation in the crystal lattice. The crystal structure of $Li_2{\cdot}(\mathbf{3})_2$ displays both tridentate monoanions $[S(H)C(PPh_2S)_2]^-$ bonded to two bridging, four-coordinate Li^+ cations (Figure 1a) in a manner similar to the Hg(II) complex $[Hg\{(Se)C(PPh_2Se)_2\}]_2$, which contains the dianionic ligands $[(Se)C(PPh_2Se)_2]^{2-}$ (**1Se**).[9] The P−S bond lengths of ca. 1.97 Å in $Li_2{\cdot}(\mathbf{3})_2$ (Table 1) are comparable with, for example, those typically observed for the dianionic ligands **1S** and **2S** in various metal complexes,[8,11,12] and the Li−S contacts of 2.406(5)-2.489(5) Å are similar to those observed in the Li^+ salts of **1S** and **2S**.[8] Most distinctly, however, the four-coordination of the PCP carbon atom is apparent in the P−C and S−C bond lengths of ca. 1.85 and 1.83 Å, respectively, that are ca. 0.1 Å longer than the analogous contacts in the ligands **1S** and **2S** with three-coordinate carbon centres. We also note that the bond parameters in the monoprotonated monoanion **3** agree well with those in the neutral half of the monoanionic ligand $[(SPh_2P)_2CSS(H)C(PPh_2S)_2]^-$, i.e. the monoprotonated derivative of **2S**, which is formally

constructed from the radical anion $[(S)C(PPh_2S)_2]^{\bullet-}$ and the neutral monoprotonated radical $[S(H)C(PPh_2S)_2]^{\bullet}$ through a central S−S bond.[8]

Synthesis and structural characterization of the Zn(II) complex $[Zn\{S(H)C(PPh_2S)_2\}_2]$ (4). Following our earlier report of the formation of the homoleptic Zn(II) complex **4** from treatment of the dimeric dianion **2S** with $ZnCl_2$,[10] the reaction of $Li_2{\cdot}(\mathbf{3})_2$ with $ZnCl_2$ in toluene was performed (Eq. 3). The complex **4** was isolated as a white powder in excellent yield (85%).

$$[Li\{S(H)C(PPh_2S)_2\}]_2{\cdot}(C_7H_8) + ZnCl_2 \rightarrow [Zn\{S(H)C(PPh_2S)_2\}_2] + 2\,LiCl + C_7H_8 \qquad (3)$$

4

The ^1H NMR spectrum of **4** in CD_2Cl_2 at 23 °C exhibits a set of multiplets in the range of 7.12-8.02 ppm and a triplet at 5.08 ppm with a coupling constant of 9.9 Hz consistent with two-bond $^2J(^1H,^{31}P)$ coupling in the P(S)C(H)P bridging unit. The $^{31}P\{^1H\}$ NMR spectrum displays a singlet at 53.7 ppm indicating a single environment for the phosphorus centres in solution.

The crystal structure of the homoleptic Zn(II) complex **4** is illustrated in Figure 1b. The compound displays a distorted octahedral coordination around the metal centre with significantly shorter Zn−S(C) bond lengths of 2.274(1) Å compared to those of the almost equal Zn−S(P) distances of 2.842(1) and 2.884(1) Å (Table 1). Furthermore, the Zn−S contacts around the metal centre in **4** are noticeably different from the Zn−S distances of 2.50-2.55 Å found for the previously reported octahedral zinc centres with homoleptic sulfur ligands.[17] These observations are consistent with considerable localization of the negative charge on the C−S unit in the monoanionic ligand **3**. The relatively weak Zn−S(P) contacts in **4** are accommodated with ca. 0.1 Å stronger P−S bonds compared to, for example, the homoleptic $[Zn\{N(P^iPr_2S)_2\}_2]$ and $[Zn\{(H)C(PPh_2S)_2\}_2]$ complexes

with four-coordinate Zn(II) centres in which the Zn−S(P) contacts of 2.35 Å give rise to P−S bond lengths of 2.05 Å.[16,18] Similarly to the Li^+ salt $Li_2{\cdot}(\mathbf{3})_2$, the Csp^3−S bond length of 1.816(4) Å and the Csp^3−P distances of ca. 1.85 Å in **4** are 0.08 and 0.1 Å longer, respectively, than in the various complexes of the dianionic ligands **1S** and **2S** reflecting the four-coordinate carbon centre in the bridging P(S)C(H)P unit of the monoanion **3** vs. the corresponding three-coordinate carbon centre in **1S** and **2S**.[8,11,12] The S−Zn−S bond angles in the range 83.8-96.2° show slightly more pronounced distortion compared to the analogous S−Ni−S angles in the octahedral Ni(II) complex **5a** (*vide infra*).

Synthesis of the Ni(II) complex $[Ni\{S(H)C(PPh_2S)_2\}_2]$ (5) and crystal structures of the octahedral and square-planar isomers 5a and 5b. As a further illustration of the synthetic potential of the monoanion **3**, the homoleptic Ni(II) complex **5** was produced by utilizing the lithium complex $Li_2{\cdot}(\mathbf{3})_2$ in a reaction with $NiCl_2$ in toluene (Eq. 4) to give complex **5** as an olive-green powder in excellent yield (93%).

$$[Li\{S(H)C(PPh_2S)_2\}]_2{\cdot}(C_7H_8) + NiCl_2 \rightarrow [Ni\{S(H)C(PPh_2S)_2\}_2] + 2\,LiCl + C_7H_8 \qquad (4)$$

5

The ^1H NMR spectrum of the green product in CD_2Cl_2 at 23 °C exhibits a set of multiplets in the range of 7.28-8.08 ppm for the C_6H_5 groups and, in contrast to the triplet observed for the Zn(II) complex **4**, *a broad singlet* at 6.16 ppm attributed to the P(S)C(H)P hydrogen atom indicating a possible fluxionality in solution. The $^{31}P\{^1H\}$ NMR spectrum displays a singlet at 51.3 ppm suggesting a single environment for the phosphorus centres at room temperature.

The crystal structures of the isomers **5a** and **5b** are shown in Figure 2. In both compounds, the asymmetric unit contains a one-half molecule of [Ni{S(H)C(PPh_2S)$_2$}$_2$] and, in the case of **5a**, a molecule of toluene solvate. In the octahedral isomer **5a** the centrosymmetric molecule is comprised of two monoanionic ligands **3** coordinated to the nickel centre in a tridentate (S,S′,S″) fashion with slightly distorted S−Ni−S bond angles in the range 87.1-92.9^o (Table 1). Most notably, *three* distinctly different Ni−S bond lengths are observed for the complex **5a**; analogously to the Zn(II) complex **4**, the sulfur atom bonded to the carbon centre forms the strongest contact to the Ni(II) centre (2.349(1) Å), whereas the two weakly coordinated thiophosphinoyl functionalities in **5a** are markedly inequivalent with Ni−S(P) distances of 2.450(1) and 2.595(1) Å. In contrast to the octahedral geometry in **4** and **5a**, a distorted square-planar geometry is apparent around the nickel atom in **5b** with S−Ni−S bond angles of 85.3 and 94.7^o (Table 1). Predictably, the protonated ligand **3** displays significantly stronger bonds to the four-coordinate Ni(II) centre in the isomer **5b** compared to the six-coordinate nickel atom in **5a**; the almost equal Ni–S bond lengths of 2.165(2) and 2.195(2) Å in **5b** are ca. 0.29 Å shorter than the mean value in **5a**. The Csp^3–S bond length of 1.846(6) Å in **5b** is significantly longer than the corresponding distance of 1.797(3) Å in **5a** reflecting the elongated Ni−S(C) bond in the latter isomer. As expected, the P−S bond length of 1.952(2) Å for the dangling Ph_2P=S group in **5b** is shorter (by ca. 0.05 Å) than the coordinated Ph_2P−S functionality. The comparatively short distances for the coordinated P−S groups in **5a** (1.970(1) and 1.962(1) Å) presumably reflect the relatively weak attachment of these sulfur atoms to the Ni(II) centre in the octahedral complex (*vide supra*).

Structural dichotomy: spectroscopic and powder X-ray diffraction studies of the isomers 5a and 5b. Interestingly, the $^{31}P\{^1H\}$ NMR spectrum of the olive-green powder **5** in CD_2Cl_2 at 23 ^{o}C shows *a singlet* at 51.3 ppm. In an attempt to understand the significance of this observation variable

temperature $^{31}P\{^{1}H\}$ NMR spectra were recorded (Figure 3). Upon cooling the solution, this singlet first broadens and then divides into two well-separated resonances at 42.8 and 68.0 ppm with equal intensity. Two broad signals are clearly evident at -40 ^{o}C and they become well-resolved at -95 ^{o}C. At this temperature the resonance at δ 42.8 appears as a doublet with a coupling constant of ca. 20 Hz consistent with a two-bond $^{2}J(^{31}P,^{31}P)$ coupling,[19] however the broadness of the resonance at δ 68.0 obscures this small coupling. Thus the low temperature $^{31}P\{^{1}H\}$ NMR spectrum of the green product suggests the sole presence of the SP isomer **5b** with two markedly different phosphorus environments.

In order to provide support for this interpretation, the ^{31}P CP/MAS NMR spectrum and the powder X-ray diffraction pattern of the olive-green product were measured. The solid-state ^{31}P NMR spectrum displays two broad isotropic signals at 46.4 and 64.4 ppm accompanied by spinning side bands consistent with the crystal structure of **5b** (Figure 4). Significantly, the powder X-ray diffraction (XRPD) pattern of the olive-green product can be perfectly indexed and fitted by the Pawley refinement method ($\chi 2$= 1.40 with 413 reflections) with the unit cell and space group settings corresponding to that determined for the single-crystal structure of the square-planar isomer **5b** without any residual unindexed diffraction profiles left in the pattern (see Figure S1 in ESI). Taken together the NMR and XRPD data indicate strongly that the olive-green product exists as the four-coordinate SP isomer **5b** in both the solid-state and in solution at low temperatures. We note that the olive-green colour of the powder is in contrast to the red-brown colour of crystalline samples of **5b** under microscope (*vide supra*).

The changes in the solution $^{31}P\{^{1}H\}$ NMR spectra of **5b** in CD_2Cl_2 at various temperatures are reversible, i.e. the singlet at 51.3 ppm reappears when the solution is warmed up to room temperature. However, this singlet is off-centred compared to the average value of 55.5 ppm observed for the two resonances at low temperature, which rules out a simple two-site exchange

process between the inequivalent phosphorus atoms of the SP isomer **5b**. The possible involvement of other structural isomers must, therefore, be considered (*cf.* DFT calculations below). In that connection paramagnetically-shifted high-field resonances were not observed in the $^{31}P\{^{1}H\}$ NMR spectra (up to -1100 ppm) in the temperature range +23 ^{o}C to -50 ^{o}C, which excludes the presence of the tetrahedral (T_d) isomer. For comparison, ^{31}P chemical shifts in the range -437 to -725 ppm have been reported for T_d $[Ni\{N(PR_2S)_2\}_2]$ (R = ^{i}Pr, Ph) complexes which incorporate a comparable, PNP-bridged sulfur-centred monoanion.[20] This observation also suggests that the O_h isomer, if it is present in solution at room temperature, is in the singlet rather than triplet ground state.

DFT calculations of the Ni(II) isomers 5a and 5b. In view of the possible octahedral – square-planar equilibrium, a series of DFT calculations were carried out. Singlet and triplet state geometries were optimized starting from both the octahedral and square-planar crystal structures and are summarized in Figure 5. In contrast to the absence of triplet state geometries *in solution* as suggested by the NMR experiments, the *solid-state* structural parameters of the octahedral geometry **5a** are reasonably well reproduced by the calculation when confining the spin-state to a triplet. Likewise, the geometric parameters optimized for the square-planar isomer **5b** are in good agreement with the experimental values when optimized in a singlet state thus suggesting that in the solid-state **5a** is in a triplet state and **5b** in a singlet state in accordance with the crystal field theory. If the square-planar geometry is relaxed into the triplet state, the optimization results in a severely distorted tetrahedral structure **5c**. On the other hand, if the octahedral geometry is relaxed into the singlet state the resulting geometry, **5b'**, closely resembles the square-planar geometry with the non-coordinated terminal thiophosphinoyl functionalities rotated towards the Ni(II) centre (see Figure 5). The free energies of the octahedral triplet (**5a**) and square-planar singlet (**5b**) are almost equal with **5a** lying only 1.09 kJ mol^{-1} lower in energy. Geometries **5b'** and **5c** are located 15.27 kJ mol^{-1} and

18.09 kJ mol^{-1} above **5b** on the free energy surface, respectively. For all geometries considered, the potential energy surface is extremely shallow and convergence criteria almost up to numerical precision had to be used to obtain fully converged geometries. Furthermore, the energy differences are fairly small and show considerable dependence on the choice of solvent model, exchange–correlation functional and basis set. All this considered, the conclusions that can be drawn from the calculated energetics is that all four geometries lie very close to each other in energy and a relatively small perturbation can induce a non-negligible change in the energetics.

In order to obtain further insight into the temperature-dependent behaviour of the $^{31}P\{^{1}H\}$ NMR spectrum, the chemical shifts of the P atoms in the singlet state geometries **5b** and **5b'** were calculated using the gauge-independent atomic orbital (GIAO) formalism. Since no paramagnetic shift was experimentally observed, the triplet geometries **5a** and **5c** were excluded from the calculations. The chemical shifts of the two equivalent phosphorus atoms were averaged in both systems. The calculated chemical shifts (relative to phosphoric acid) show values of δ 36.5 and 52.0 for **5b** and δ 31.6 and 47.9 for **5b'** in qualitative agreement with the low- temperature experimental chemical shifts of 42.8 and 68.0 ppm. It should be noted that NMR shifts are a challenging property to calculate especially for heavier elements and moderate errors in the absolute values are typically seen − especially when an external reference is used. The relative values of the chemical shifts should, however, be reliable.

The experimental $^{31}P\{^{1}H\}$ NMR spectrum can be rationalized by assuming that the singlet geometries **5b** and **5b'** exist in a dynamic equilibrium at room temperature whereas only the lower energy singlet isomer **5b** exists at lower temperatures. Consequently, there are four possible chemical environments at ambient temperatures for the P atoms – two in **5b** and two in **5b'**. A four-site dynamic exchange process would then average out the four calculated chemical shifts to 42.0 ppm, which is shifted slightly upfield compared to the average of the two calculated values for **5b**

(44.3 ppm). This is in good qualitative agreement with the experimental observation that the room temperature singlet is observed at 51.3 ppm, which is slightly upfield from the average value of the two signals observed at low temperature (55.5 ppm).

UV-Vis spectroscopy of the Ni(II) isomers 5. The electronic spectra of **5a**, **5b**, **5b'** and **5c** were calculated with time-dependent DFT (TDDFT) including the fifty lowest excitations. The UV-Vis spectrum simulated from the calculated excitation wavelengths and oscillator strengths along with the experimental spectrum of **5b** is presented in Figure S2 and the numerical values are given in Table S2 (*cf.* ESI). Based on the calculations, the measured spectra cannot be unambiguously assigned to any specific isomer. Both of the singlet geometries (**5b** and **5b'**) show one major absorption peak at 280 nm and 278 nm, respectively, corresponding to a ligand-to-metal charge transfer excitation. It is also noteworthy that the absorption bands of these two isomers overlap almost perfectly. Therefore, the **5b**–**5b'** equilibrium suggested by the low temperature $^{31}P\{^{1}H\}$ NMR measurements cannot be observed in the corresponding variable temperature UV-Vis spectra. Indeed, the main absorption band in the experimental spectra is shifted only by 8 nm when the temperature is lowered from ambient conditions to –50 C° (Figure S3).

Conclusions

In order to pursue investigations of the chemistry of M(II) complexes **4** and **5** (M = Zn, Ni), a high-yield synthesis of the new reagent $[Li\{S(H)C(PPh_2S)_2\}]_2$ $[Li_2\cdot(\mathbf{3})_2]$ was developed. This important advancement opens the way for extensive studies of the coordination behaviour of this potentially versatile, sulfur-centred ligand in main group, transition-metal and lanthanide complexes for comparison with that of the corresponding dianion **1S**.[10]

The novel monoanionic ligand **3** adopts a distorted octahedral coordination around the metal centre in the homoleptic Zn(II) complex **4** with unusually weak Zn−S(P) contacts. Significantly, the first example of structurally characterized six- and four-coordinate isomers of a nickel(II) complex (**5a** and **5b**) with the same ligand, viz. $[S(H)C(PPh_2S)_2]^-$, was discovered. DFT calculations display virtually no difference between the energies of **5a** and **5b** in solution. Consistently, detailed NMR investigations indicate that a mixture of singlet state isomers persists in solution at room temperature, while the square-planar isomer **5b** prevails at -40 ^oC as well as in the solid-state. In addition, the isomerization process was shown to be specific to the Ni(II) complex, since no splitting of the singlet in $^{31}P\{^1H\}$ NMR spectrum of the Zn(II) complex **4** was observable even at -90 ^oC. Additional studies are in progress in order to elucidate the redox properties of the homoleptic Ni(II) complex **5** in the context of the similarity of the Ni−S coordination to ligand environments in the active sites of certain redox-active nickel enzymes.

Experimental Section

Reagents and general procedures: All reactions and the manipulations of products were performed under an argon atmosphere by using standard Schlenk techniques or an inert atmosphere glove box. The compounds $[H_2C(PPh_2)_2]$ (Strem Chemicals, 97%), MeLi (Aldrich, 1.6 M sol. in Et_2O), ^nBuLi (Aldrich, 2.5 M sol. in hexanes) and $NiCl_2$ (Merck, 99.995%) were used as received. $[H_2C(PPh_2S)_2]$ and $[\{Li(TMEDA)\}_2\{(S)C(PPh_2S)_2\}]$ were prepared as reported earlier.[8] The solvents CH_2Cl_2, toluene and Et_2O were dried with a MBraun MB-SPS800 solvent purification system operating under argon atmosphere. Elemental analyses were performed by analytical services at the Department of Chemistry, University of Calgary [compound **5a**·$(C_7H_8)_2$] and at the Department of Chemistry, University of Jyväskylä [compounds Li_2·(**3**)$_2$, **4** and **5b**].

Spectroscopic methods: The ^{1}H, ^{7}Li and $^{31}P\{^{1}H\}$ NMR spectra were obtained in CD_2Cl_2 at 23 ºC on a Bruker Avance III 300 spectrometer operating at 300.15, 116.65 and 121.52 MHz, respectively. The solid-state and variable temperature NMR measurements were performed on Bruker Avance 400 and Bruker Avance DRX 500 spectrometers, respectively. ^{1}H NMR spectra are referenced to the solvent signal and the chemical shifts are reported relative to $(CH_3)_4Si$. The ^{7}Li and $^{31}P\{^{1}H\}$ NMR spectra are referenced externally and the chemical shifts are reported relative to a 1.0 M solution of LiCl in D_2O and to an 85% solution of H_3PO_4 in D_2O, respectively. The UV-Vis spectra of $[Ni\{S(H)C(PPh_2S)_2\}_2]$ (**5b**) were measured with PerkinElmer Lambda 650 (at 23 ºC) and 900 (at -50 ºC) spectrophotometers in CH_2Cl_2.

X-ray crystallography: Crystallographic data for compounds $Li_2{\cdot}(\mathbf{3})_2$, **4**, **5a**$\cdot(C_7H_8)_2$ and **5b** are summarized in Table 2. Crystals of $[Li\{S(H)C(PPh_2S)_2\}]_2$ $[Li_2{\cdot}(\mathbf{3})_2]$, $[Zn\{S(H)C(PPh_2S)_2\}_2]$ (**4**), octahedral $[Ni\{S(H)C(PPh_2S)_2\}_2{\cdot}(C_7H_8)_2]$ [**5a**$\cdot(C_7H_8)_2$] and square-planar $[Ni\{S(H)C(PPh_2S)_2\}_2]$ (**5b**) were coated with Paratone 8277 [**5a**$\cdot(C_7H_8)_2$] or Fomblin® Y [$Li_2{\cdot}(\mathbf{3})_2$, **4** and **5b**] oil and mounted on a glass fibre or a MiTeGen loop. Diffraction data were collected on a Bruker-Nonius Kappa APEX II CCD diffractometer using monochromated MoKα radiation (λ = 0.71073 Å) at -100 °C [**5a**$\cdot(C_7H_8)_2$] or at –150 °C (**5b**), and on an Agilent SuperNova Dual Source diffractometer equipped with Atlas CCD area-detector using graphite monochromatized CuKα radiation (λ = 1.54184 Å) at –150 °C [$Li_2{\cdot}(\mathbf{3})_2$ and **4**]. The data were processed by applying an empirical absorption correction with DENZO-SMN v0.93.0 program for compounds **5a**$\cdot(C_7H_8)_2$ and **5b**, and by performing an analytical numeric absorption correction using a multifaceted crystal with CrysAlis^{Pro} program for compounds $Li_2{\cdot}(\mathbf{3})_2$ and **4**. All structures were solved by direct methods with the SIR-97 or SHELXS and refined by using SHELXL programs.[21] After full-matrix least-squares refinement of the non-hydrogen atoms with anisotropic thermal parameters, the hydrogen

atoms were placed in calculated positions (C-H = 0.95 Å for -CH and 0.99 Å for -CH_2 hydrogens). The isotropic thermal parameters of the hydrogen atoms were fixed at 1.2 times that of the corresponding carbon for -CH and -CH_2 hydrogens. In the final refinement the hydrogen atoms were riding on their respective carbon atoms. CCDC 1424394 [Li_2·(**3**)], 1486829 (**4**), 1424395 [**5a**·$(C_7H_8)_2$] and 1424396 (**5b**) contain the supplementary crystallographic data for this paper. These data can be obtained free of charge from The Cambridge Crystallographic Data Centre via www.ccdc.cam.ac.uk/data_request/cif.

X-ray powder diffraction data (XRPD): The bulk powder sample of **5b** was examined by X-ray powder diffraction (XRPD) using a PANalytical X´Pert PRO diffractometer at room temperature. Primary beam Johansson monochromator was used to produce $CuK_{\alpha 1}$ radiation (1.5406 Å, 45 kV, 40 mA). Each sample was prepared on to a silicon-made sample holder (producing zero-background signal) using petrolatum jelly as an adhesive. Diffraction pattern was collected with a position sensitive X´Celerator detector in a continuous scanning mode using 2θ-range of 3-70° with a step size of 0.017° and recording time of 40 s per step. HighScore Plus (v. 4.1)[22] program was used to examine the data and the DASH program[23] for the auto-indexing (with sub-program DICVOL)[24] and whole-pattern Pawley refinement of the patterns.

Truncated 2θ-range of 5-50° with first 25 diffraction peak positions were used as an input for the auto-indexing procedure in order to search the best fitting unit cell parameters. As the result all the peaks were indexed by triclinic unit cell settings a = 12.4580(38) Å, b = 11.5306(38) Å, c = 9.3914(29) Å, α = 66.128(25)° β= 96.716(24)°, γ = 103.724(22)° and V = 1198.1 $Å^3$ with reasonable figure of merits (M_{25} = 36.7, F_{25} = 133.6 (0.0060, 31).[25] Prior to Pawley refinement *P*-1 space group was assigned based on the settings determined by single-crystal analysis, and the unit cell settings afforded by the indexing were converted to correspond settings of the single-crystal structure.

Extraction of individual diffraction intensities by Pawley refinement process lead to good agreement between observed and calculated pattern with χ^2 = 1.40 (413 reflections; R_{wp} = 14.95 % and R_{exp}= 12.63 %) with refined unit cell setting shown in the Table S1 (see ESI).

Computational details. All geometry optimizations, frequency calculations, stability analyses and TDDFT calculations were performed with Gaussian 09 revision D.01[26] using the LC-ωPBE range-separated hybrid functional[27] and def2-TZVP basis sets[28]. This functional was chosen due to its good ability to predict relative energies of different spin states[29]. The geometries of **5a**, **5b**, **5b'** and **5c** were fully optimized in both low- and high-spin states with no constraints placed on spatial or spin symmetries. Due to the flat nature of the potential energy surfaces the Gaussian "VeryTight" convergence criteria and "UltraFine" integration grid were used to ensure that the bottoms of potential energy minima were correctly located. Using looser convergence criteria leads to differences of several kJ mol^{-1} in the relative energies between the calculated geometries and can even affect the relative ordering of the geometries. The low-spin states show no spin-contamination and stability analysis was performed on the solutions to ensure that no lower energy broken symmetry states exist. It should be noted that if a conventional global hybrid (such as B3LYP[30]) is used, the low-spin solutions break symmetry and show noticeable spin-contamination with partial delocalization of the spin density into the ligand sulfur atoms. Such an effect is also observed with the LC-ωPBE functional if smaller basis sets (such as 6-31G(d,p)[31]) are used. Frequency calculations were carried out to ensure that the stationary geometries correspond to minima on the potential energy surface. Solvent effects were taken into account in the geometry optimizations, frequency calculations and TDDFT calculations with the polarizable continuum model (PCM) using the default parameters for CH_2Cl_2 as implemented in Gaussian 09. Same level of theory as for the

geometry optimizations and frequency calculations was used for the TDDFT calculations. Fifty lowest roots were solved for all four isomers.

^{31}P NMR shifts of **5b** and **5b'** were calculated using the gauge-independent atomic orbital (GIAO) formalism[32] as implemented in the ADF 2014 program package[33]. Because the LC-ωPBE functional is not available in ADF the PBE0 global hybrid functional[34] was used instead. The LC-ωPBE/def2-TZVP-optimized geometries were used in the NMR calculations. Scalar relativistic effects were included using the zeroth order regular approximation (ZORA)[35]. Standard ZORA-TZ2P basis sets[36] as implemented in the ADF basis set library were used for atoms other than phosphorus. For P atoms special JCPL basis[37] was used, which includes the same functions as the corresponding TZ2P basis but is augmented with four additional steep s functions to offer more flexibility in the core region. The relative shifts were calculated using phosphoric acid as a reference. The reference geometry and shifts were calculated using an identical procedure as for **5b** and **5b'**.

Synthesis of [Li{S(H)C(PPh$_2$S)$_2$}]$_2$ [Li$_2$·(3)$_2$]. A solution of [H$_2$C(PPh$_2$S)$_2$] (0.449 g, 1.00 mmol) in 20 mL of toluene was cooled to -80 ^{o}C and 0.40 mL of ^{n}BuLi solution (2.5 M in hexanes, 1.00 mmol) was added by syringe. The reaction mixture was stirred for 5 min at -80 ^{o}C and 2 h at 23 ^{o}C. The resulting pale yellow solution was added dropwise to a solution of S_8 (0.032 g, 1.00 mmol) in 10 mL of toluene at 23 ^{o}C and stirring was continued for 2 h resulting in a very pale yellow powder. The product was allowed to settle and the solution was decanted via cannula followed by washing with toluene (2×30 mL) affording [Li{S(H)C(PPh$_2$S)$_2$}]$_2$·(C$_7$H$_8$) [Li$_2$·(**3**)$_2$·(C$_7$H$_8$)] as a toluene solvate (0.479 g, 90%). Anal. Calcd (%) for $C_{57}H_{50}Li_2P_4S_6$: C, 64.30; H, 4.73 Found: C, 64.40; H, 4.69 %. ^{1}H NMR (CD$_2$Cl$_2$, 23 ^{o}C): δ 6.89-8.07 [m, 45H, C$_6$*H*$_5$ of Ph groups and toluene], δ 5.18 [t, 2H, PC(*H*)P, $^2J(^1H,^{31}P)$ = 7.5 Hz], δ 2.33 [s, 3H, C*H*$_3$ of toluene]; ^{7}Li NMR: δ 1.44; ^{31}P{^{1}H} NMR:

δ 53.1. X-ray quality crystals were obtained from the CH_2Cl_2 solution of $[Li_2{\cdot}(\mathbf{3})_2]{\cdot}(C_7H_8)$ after 4 days at -20 ^oC; the colourless plates did not contain the toluene solvate present in the original product powder.

Synthesis of [Zn{S(H)C(PPh$_2$S)$_2$}$_2$] (4). A mixture of $[Li\{S(H)C(PPh_2S)_2\}]_2{\cdot}(C_7H_8)$ $[Li_2{\cdot}(\mathbf{3})_2{\cdot}(C_7H_8)]$ (0.533 g, 0.50 mmol) and $ZnCl_2$ (0.068g, 0.50 mmol) powders was dissolved to 20 mL of toluene and the reaction mixture was stirred for 3 h at 65 ^oC. The product was allowed to settle and the solution was decanted via cannula followed by further washing with toluene (2 × 20 mL) affording of $[Zn\{S(H)C(PPh_2S)_2\}_2]$ (**4**) as a white powder (0.435 g, 85%). Anal. Calcd (%) for $C_{50}H_{42}P_4S_6Zn$: C, 58.62; H, 4.13. Found: C, 58.16; H, 4.03. ^1H NMR (CD_2Cl_2, 23 °C): δ 7.12-8.02 [m, 40, C_6H_5 of Ph groups], 5.08 [t, 2H, PC(*H*)P, $^2J(^1H,^{31}P)$ = 9.9 Hz]; $^{31}P\{^1H\}$ NMR (CD_2Cl_2, 23 °C): δ 53.7 (s). X-ray quality crystals were obtained by slow diffusion from the CH_2Cl_2 solution of **4** layered with Et_2O after 2 days at +4 ^oC.

Synthesis of [Ni{S(H)C(PPh$_2$S)$_2$}$_2$] (5b). A solution of $[H_2C(PPh_2S)_2]$ (0.449 g, 1.00 mmol) in 20 mL of toluene was cooled to -80 ^oC and 0.40 mL of ^{n}BuLi solution (2.5 M in hexanes, 1.00 mmol) was added by syringe. The reaction mixture was stirred for 5 min at -80 ^oC and 2 h at 23 ^oC. The resulting pale yellow solution was added dropwise to a mixture of S_8 (0.032 g, 1.00 mmol) and $NiCl_2$ (0.065 g, 0.50 mmol) in 20 mL of toluene at 23 ^oC. The reaction mixture was stirred for 3 h at 75 ^oC resulting in an olive-green powder. The product was allowed to settle and the solution was decanted via cannula followed by washing with toluene and THF (2 × 20 mL of each solvent) affording of $[Ni\{S(H)C(PPh_2S)_2\}_2]$ (**5b**) as a green powder (0.474 g, 93%). Anal. Calcd (%) for $C_{50}H_{42}NiP_4S_6$: C, 59.03; H, 4.16; Found: C, 58.83; H, 4.00. ^1H NMR (CD_2Cl_2, 23 ^oC): δ 7.28-8.08 [m, 40H, C_6H_5], δ 6.16 [br, s, 2H, PC(*H*)P]; $^{31}P\{^1H\}$ NMR (CD_2Cl_2, 23 ^oC): δ 51.3. UV-Vis (23 ^oC,

CH_2Cl_2): 272 nm (ε = 2.4 × 10^4 $M^{-1}cm^{-1}$), 336 nm (ε = 2.2 × 10^4 $M^{-1}cm^{-1}$), 515 nm (ε = 4.9 × 10^2 $M^{-1}cm^{-1}$) and 695 nm (ε = 4.8 × 10^2 $M^{-1}cm^{-1}$). UV-Vis (-50 °C, CH_2Cl_2): 328 nm (ε = 2.3 × 10^4 $M^{-1}cm^{-1}$).

Formation of octahedral [Ni{S(H)C(PPh$_2$S)$_2$}$_2$·(C$_7$H$_8$)$_2$] [5a·(C$_7$H$_8$)]. [Li_2{(S)C($PPh_2S)_2$}] (0.67 mmol, prepared *in situ* from 0.300 g of [$H_2C(PPh_2S)_2$], 0.84 mL of 1.6 M MeLi and 0.021g of S_8)[8] in toluene (20 mL) was added to a suspension of $NiCl_2$ (0.087 g, 0.67 mmol) in toluene (5 mL) at -80 °C and stirred for 15 min. The reaction mixture was allowed to reach room temperature and stirring was continued for an additional 12 h. The LiCl precipitate was removed by filtration and the greenish brown filtrate was kept in a glove box at room temperature for slow evaporation of solvent. Dark green crystals were isolated, washed with benzene and dried by prolonged pumping under vacuum. Yield: 0.042 g (12%). Characterization data for **5a**·C_7H_8: Anal. Calcd (%) for $C_{57}H_{50}NiP_4S_6$: C, 61.68; H, 4.54. Found: C, 61.48; H, 4.70. $^{31}P\{^1H\}$ NMR (CD_2Cl_2, 23 °C): δ 51.2 (s, br). ^1H NMR (CD_2Cl_2, 23 °C): δ 7.24-8.08 [m, 45H, C_6H_5 of Ph groups and toluene], 6.16 [br, s, 2H, PC(*H*)P], 2.32 [s, 3H, CH_3 of toluene]. Crystals of **5a**·(C_7H_8)$_2$ were obtained by slow evaporation of a toluene solution under argon.

Acknowledgments

The authors gratefully acknowledge financial support from the Natural Sciences and Engineering Research Council, Canada (RT, TC) and the Academy of Finland. We are grateful to Adjunct Prof. Elina Sievänen, Mr. Esa Haapaniemi and Mr. Antti Sinikangas (University of Jyväskylä) for recording the VT and CP/MAS NMR spectra, and to Dr. Pasi Myllyperkiö for conducting the low temperature UV-Vis measurements (Nanoscience Center, University of Jyväskylä).

References

1 (a) T. Cantat, N. Mezailles, L. Ricard, Y. Jean and P. Le Floch, *Angew. Chem. Int. Ed.*, 2004, **43**, 6382-6385; (b) T. Cantat, L. Ricard, Y. Jean, P. Le Floch and N. Mezailles, *Organometallics*, 2006, **25**, 4965-4976.

2 M. F. Boutignon, H. Heuclin, X. F. Le Goff and N. Mézailles, *Chem. Commun*., 2012, **48**, 3306-3308, and references therein.

3 For recent reviews, see (a) S. T. Liddle, D. P. Mills and A. J. Wooles, *Chem. Soc. Rev*., 2011, **40**, 2164-2176; (b) T. Cantat, N. Mézailles, A. Auffrant and P. Le Floch, *Dalton Trans*., 2008, 1957-1972.

4 For examples of actinide complexes see, (a) J-C. Tourneux, J-C. Berthet, T. Cantat, P. Thuéry, N. Mézailles and M. Ephritikhine, *J. Am. Chem. Soc*., 2011, **133**, 6162-6165; (b) J-C. Tourneux, J-C. Berthet, T. Cantat, P. Thuéry, N. Mézailles, P. Le Floch and M. Ephritikhine, *Organometallics*, 2011, **30**, 2957-2961; (c) T. Cantat, A. Noël, P. Thuéry, M. Ephritikhine, P. Le Floch and N. Mézailles, *J. Am. Chem. Soc*., 2009, **131**, 963-972.

5 For examples of p-block metal complexes see, (a) R. Thirumoorthi, T. Chivers and I. Vargas-Baca, *Dalton Trans*., 2011, **40**, 8086-8088; (b) W.-P. Leung, C.-L. Wan, K.-W. Kan and T. C. W. Mak, *Organometallics*, 2010, **29**, 814-820.

6 S. T. Liddle, D. P. Mills and A. J. Wooles, *Organomet. Chem.*, 2010, **36**, 29-55.

7 D. J. Mindiola and J. Scott, *Nat. Chem.*, 2011, **3**, 15-17.

8 J. Konu, T. Chivers and H. M. Tuononen, *Chem. Eur. J.*, 2010, **16**, 12977-12987.

9 J. Konu and T. Chivers, *Chem. Commun.*, 2010, **46**, 1431-1433.

10 For a review, see T. Chivers, J. Konu and R. Thirumoorthi, *Dalton Trans.*, 2012, **41**, 4283-4295.

11 (a) M. Risto, T. Chivers and J. Konu, *Dalton Trans.*, 2011, **40**, 8238-8246; (b) R. Thirumoorthi, T. Chivers and I. Vargas-Baca, *Organometallics*, 2012, **31**, 627-636; (c) R. Thirumoorthi and T. Chivers, *Z. Anorg. Allg. Chem*., 2014, **640**, 23-26.

12 (a) J. Konu, T. Chivers and H.M. Tuononen, *Chem. Eur. J.*, 2011, **17**, 11844-11856; (b) M. Risto, J. Konu and T. Chivers, *Inorg. Chem*., 2011, **50**, 406-408.

13 E. Ferentinos, D. Maganas, C. P. Raptopoulou, A. Terzis, V. Psycharis, N. Robertson and P. Kyritsis, *Dalton Trans.*, 2011, **40**, 169-180.

14 Four-coordinate square-planar and tetrahedral stereoisomers are well-known for Ni(II) complexes, e.g. [Ni{(SeP^iPr_2)$_2$N}$_2$], N. Levesanos, S. D. Robertson, D. Maganas, C. P. Raptopoulou, A. Terzis, P. Kyritsis and T. Chivers, *Inorg. Chem.*, 2008, **47**, 2949-2951.

15 The monoanionic ligand in [Li{HC(PPh_2S)$_2$}(THF)(Et_2O)] is *S,S'*-chelated to a bis-solvated Li centre, W-P. Leung, C-L. Wan, T. C. W. Mak, *Organometallics*, 2010, **29**, 1622-1628.

16 Heavier alkali-metal derivatives of [HC(PPh_2S)$_2$]$^-$ have also been prepared from $H_2C(PPh_2S)_2$ via alkane elimination reactions. R. Thirumoorthi and T. Chivers, *Eur. J. Inorg. Chem.*, 2012, 3061-3069.

17 Only 5 entries of octahedral zinc centres with homoleptic sulfur ligands are deposited in the Cambridge Crystallographic Data Centre (May 2016): (a) T. Sugaya, T. Fujihara, A. Nagasawa and K. Unoura, *Inorg. Chim. Acta*, 2009, **362**, 4813-4822; (b) M.L Helm, C.M. Combs, D.G. Van der Veer and G. J. Grant, *Inorg. Chim Acta*, 2002, **338**, 182-188; (c) G. Sakane, H. Kawasaki, T. Oomori, M. Yamasaki, H. Adachi and T. Shibahara, *J. Cluster Sci.*, 2002, **13**, 75-102; (d) H.-J. Kuppers, K. Wieghardt, B. Nuber and J. Weiss, *Z. Anorg. Allg. Chem.*, 1989, **577**, 155-161; (e) W.N. Setzer, Q. Guo, G.J. Grant, J.L. Hubbard, R.S. Glass and D.G. Van der Veer, *Heteroatom Chem.*, 1990, **1**, 317-320.

18 (a) D. Cupertino, R. Keyte, A. M. Z. Slawin, D. J. Williams and J. D. Woollins, *Inorg. Chem.*, 1996, **35**, 2695-2697; (b) M. Afzaal, D. Crouch, M. A. Malik, M. Motevalli, P O'Brien, J.-H. Park and J. D. Woollins, *Eur. J. Inorg. Chem.*, 2004, 171-177; (c) S. Schulz, R. Schaper, D. Blaser and C. Wolper, *Z. Anorg. Allg. Chem.*, 2012, **638**, 2102-2105.

19 J.-H. Chen, J. Guo, Y. Li and C.-W- So, *Organometallics*, 2009, **28**, 4617-4620.

20 (a) E. Simon-Manso, M. Valderrama and D. Boys, *Inorg. Chem.*, 2001, **40**, 3647-3649; (b) D. Maganas, A. Grigoropoulos, S. S. Staniland, S. D. Chatziefthimiou, A. Harrison, N. Robertson, P. Kyritsis and F Neese, *Inorg. Chem.*, 2010, **49**, 5079-5093.

21 (a) A. Altomare, M. C. Burla, M. Camalli, G. L. Cascarano, C. Giacovazzo, A. Guagliardi, A. G. G. Moliterni, G. Polidori and R. Spagna, *J. Appl. Crystallogr.*, 1999, **32**, 115–119; (b) G. M. Sheldrick, *Acta Crystallogr., Sect. A: Fundam. Crystallogr.*, 2008, **64**, 112–122.

22 HighScore plus 4.1, PANalytical BV. Almelo, Netherlands, 2014.

23 W. I. F. Shankland, J. van de Streek, E. Pidcock, W. D. S. Motherwell and J. C. Cole, *J. Appl. Cryst.*, 2006, **39**, 910-915.

24 A. Boultif and D. Louër, *J. Appl. Cryst.*, 2004, **37**, 724-731.

25 P. M. De Wolff, *J. Appl. Crystallogr.*, 1968, **1**, 108-113.

26 Gaussian 09, Revision D.01, M. J. Frisch, G. W. Trucks, H. B. Schlegel, G. E. Scuseria, M. A. Robb, J. R. Cheeseman, G. Scalmani, V. Barone, B. Mennucci, G. A. Petersson, H. Nakatsuji, M. Caricato, X. Li, H. P. Hratchian, A. F. Izmaylov, J. Bloino, G. Zheng, J. L. Sonnenberg, M. Hada, M. Ehara, K. Toyota, R. Fukuda, J. Hasegawa, M. Ishida, T. Nakajima, Y. Honda, O. Kitao, H. Nakai, T. Vreven, J. A. Montgomery, Jr., J. E. Peralta, F. Ogliaro, M. Bearpark, J. J. Heyd, E. Brothers, K. N. Kudin, V. N. Staroverov, R. Kobayashi, J. Normand, K. Raghavachari, A. Rendell, J. C. Burant, S. S. Iyengar, J. Tomasi, M. Cossi, N. Rega, J. M. Millam, M. Klene, J. E. Knox, J. B. Cross, V. Bakken, C. Adamo, J. Jaramillo, R. Gomperts, R. E. Stratmann, O. Yazyev, A. J. Austin, R. Cammi, C. Pomelli, J. W. Ochterski, R. L. Martin, K. Morokuma, V. G. Zakrzewski, G. A. Voth, P. Salvador, J. J. Dannenberg, S. Dapprich, A. D. Daniels, Ö. Farkas, J. B. Foresman, J. V. Ortiz, J. Cioslowski, D. J. Fox, Gaussian Inc., Wallingford CT, 2009.

27 O. A. Vydrov and G. E. Scuseria, *J. Chem. Phys.*, 2006, **125**, 234109(1-9).

28 (a) F. Weigend, M. Häser, H. Patzelt and R. Ahlrichs, *Chem. Phys. Lett.*, 1998, **294**, 143-152; (b) F. Weigend and R. Ahlrichs, *Phys. Chem. Chem. Phys.*, 2005, **7**, 3297-3305.

29 (a) P. Rivero, I. de P. R. Moreira, F. Illas and G. E. Scuseria, *J. Chem. Phys.*, 2008, **129**, 184110(1-7); (b) J. Peralta and J. I. Melo, *J. Chem. Theory Comput.*, 2010, **6**, 1894-1899; (c) E. Ruiz, *J. Comput. Chem.*, 2011, **32**, 1998-2004; (d) T. Saito, A. Ito, T. Watanabe, T. Kawakami, M. Okumura and K. Yamaguchi, *Chem. Phys. Lett.*, 2012, **542**, 19-25; (e) R. Costa, R. Valero, D. R. MaÇeru, I. de P. R. Moreira and F. Illas, *J. Chem. Theory Comput.*, 2015, **11**, 1006-1019.

30 (a) P. J. Stephens, F. J. Devlin, C. F. Chabalowski and M. J. Frisch, *J. Phys. Chem.*, 1994, **98**, 11623–11627; (b) A. D. Becke, *J. Chem. Phys.*, 1993, **98**, 5648–5652; (c) A. D. Becke, *Phys. Rev. A*, 1988, **38**, 3098–3100; (d) C. Lee, W. Yang and R. G. Parr, *Phys. Rev. B*, 1988, **37**, 785–789.

31 W. J. Hehre, R. Ditchfeld and J. A. Pople, *J. Chem. Phys.*, 1972, **56**, 2257-2261.

32 (a) S. K. Wolff, T. Ziegler, E. van Lenthe and E. J. Baerends, *J. Chem. Phys.*, 1999, **110**, 7689–7698; (b) A. Schreckenbach and T. Ziegler, *J. Phys. Chem.*, 1995, **99**, 606–611.

33 ADF2014. SCM, Theoretical Chemistry, Vrije Universiteit, Amsterdam. http://www.scm.com. 2014.

34 (a) J. P. Perdew, K. Burke and M. Ernzerhof, *Phys. Rev. Lett.*, 1996, **77**, 3865-3868; (b) J. P. Perdew, K. Burke and M. Ernzerhof, *Phys. Rev. Lett.*, 1997, **78**, 1396-1396; (c) J. P. Perdew, M. Ernzerhof and K. Burke, *J. Chem. Phys.*, 1996, **105**, 9982-9985; (d) C. Adamo and V. Barone, *J. Chem. Phys.*, 1999, **110**, 6158-6170.

35 (a) E. van Lenthe, E. J. Baerends and J. G. Snijders, *J. Chem. Phys.*, 1993, **99**, 4597-4610; (b) E. van Lenthe, E. J. Baerends and J. G. Snijders. *J. Chem. Phys.*, 1994, **101**, 9783-9792; (c) E. van Lenthe, R. van Leeuwen, E. J. Baerends and J. G. Snijders, *Int. J. Quantum. Chem.*, 1996, **57**, 281-293; (d) E. van Lenthe, J. G. Snijders and E. J. Baerends, *J. Chem. Phys.*, 1996, **105**, 6505-6516.

36 E. van Lenthe and E. J. Baerends, *J. Comp. Chem.*, 2003, **24**, 1142-1156.

37 S. Moncho and J. Autschbach, *J. Chem. Theory Comput.*, 2010, **6**, 223-234.

Table 1. Selected bond lengths (Å) and angles (°) in $[Li\{S(H)C(PPh_2S)_2\}]_2$ [$Li_2\cdot(\mathbf{3})_2$], $[Zn\{S(H)C(PPh_2S)_2\}_2]$ (**4**), octahedral $[Ni\{S(H)C(PPh_2S)_2\}_2\cdot(C_7H_8)_2]$ [**5a**$\cdot(C_7H_8)_2$] and square planar $[Ni\{S(H)C(PPh_2S)_2\}_2]$ (**5b**).

	$Li_2\cdot(\mathbf{3})_2$ [b]	**4** [c]	**5a**$\cdot(C_7H_8)_2$ [d]	**5b** [d]
M1–S1	2.489(5)	2.842(1)	2.450(1)	2.165(2)
M1–S2	2.424(5)[a]	2.884(1)	2.595(1)	-
M1–S3	2.406(5)	2.274(1)	2.349(1)	2.195(2)
P1–C25	1.838(2)	1.850(4)	1.831(3)	1.835(6)
P2–C25	1.856(2)	1.856(4)	1.826(3)	1.839(6)
S3-C25	1.825(2)	1.816(4)	1.797(3)	1.846(6)
P1–S1	1.9644(8)	1.964(1)	1.970(1)	1.997(2)
P2–S2	1.9762(8)	1.966(1)	1.962(1)	1.952(2)
S3–M1–S3[a]	113.8(2)	180	180	180
S1–M1–S1[a]	-	180	180	180
S2–M1–S2[a]	-	180	180	-
S3–M1–S1	94.9(2)	92.08(2)	91.32(3)	94.70(6)
S3[a]–M1–S1	111.5(2)	87.92(3)	88.68(3)	85.30(6)
S3–M1–S2	97.0(2)	83.83(3)	89.53(3)	-
S3–M1–S2[a]	94.5(2)	96.18(3)	90.47(3)	-
S1–M1–S2	-	84.70(3)	87.09(3)	-
S1[a]–M1–S2	144.0(2)	95.30(3)	92.91(3)	-
P2–C25–P1	120.1(1)	117.3(2)	118.7(2)	119.3(3)
S3–C25–P2	106.8(1)	109.6(2)	106.4(2)	114.5(3)
S3–C25–P1	110.3(1)	107.0(2)	105.2(2)	104.8(3)
C25–P1–S1	116.38(7)	111.4(1)	111 (1)	110.1(2)
C25–P2–S2	113.64(8)	113.8(1)	110.5(1)	112.8(2)
P1–S1–M1	100.4(1)	90.69(4)	98.46(4)	100.1(1)
P2–S2–M1	88.9 8(1)[a]	94.05(4)	97.33(5)	-

[a] Symmetry operations: 2-x, 1-y, -z in $Li_2\cdot(\mathbf{3})_2$; 1-x, 2-y, -z in **4**; -x, -y, 2-z in **5a**$\cdot(C_7H_8)_2$; -x, -y, 1-z in **5b**. [b] M = Li. [c] M = Zn. [d] M = Ni.

Table 2. Crystallographic data for $[Li\{S(H)C(PPh_2S)_2\}]_2$ $[Li_2\cdot(\mathbf{3})_2]$,[a] $[Zn\{S(H)C(PPh_2S)_2\}_2]$ (**4**),[a] octahedral $[Ni\{S(H)C(PPh_2S)_2\}_2\cdot(C_7H_8)_2]$ [**5a**$\cdot(C_7H_8)_2$],[b] and square planar $[Ni\{S(H)C(PPh_2S)_2\}_2]$ (**5b**)[b].

	$Li_2\cdot(\mathbf{3})_2$	**4**	**5a**$\cdot(C_7H_8)_2$	**5b**
emp. formula	$C_{50}H_{42}Li_2P_4S_6$	$C_{50}H_{42}P_4S_6Zn$	$C_{64}H_{58}NiP_4S_6$	$C_{50}H_{42}NiP_4S_6$
Fw	972.95	1024.44	1202.05	1017.79
cryst. system	Monoclinic	Monoclinic	Monoclinic	Triclinic
space group	$P2_1/c$	$P2_1/c$	$P2_1/n$	P-1
a, Å	10.6957(1)	10.7246(2)	11.0600(3)	9.297(5)
b, Å	18.1994(2)	18.3260(3)	15.7060(4)	11.399(5)
c, Å	11.9093(1)	11.6699(2)	16.8660(4)	12.389(5)
α, deg.	90.00	90.00	90.00	75.706(5)
β, deg.	94.0727(9)	93.746(2)	106.262(1)	83.003(5)
γ, deg.	90.00	90.00	90.00	66.213(5)
V, $Å^3$	2312.34(4)	2288.69(7)	2812.6(1)	11.63(9)
Z	2	2	2	1
T, °C	-150	-150	-100	-150
ρ_{calcd}, g/cm^3	1.397	1.487	1.419	1.452
μ(Mo Kα), mm^{-1}	4.314	4.907	0.723	0.859
crystal size, mm^3	0.09×0.06×0.03	0.31×0.08×0.03	0.26×0.23×0.13	0.10×0.06×0.02
F(000)	1008	1056	1252	526
Θ range, deg	4.14-66.97	4.13-67.68	2.36-27.00	2.45-25.02
reflns collected	12842	7806	21124	6961
unique reflns	3645	4025	6131	4097
R_{int}	0.0328	0.0309	0.0559	0.0581
reflns [$I>2\sigma(I)$]	4108	4641	5176	3001
R_1 [$I>2\sigma(I)$]	0.0369	0.0571	0.0596	0.0705
wR_2 (all data)	0.0986	0.1369	0.1440	0.1545
GOF on F^2	1.051	1.049	1.127	1.099
completeness	0.997	0.996	0.999	0.996

[a] λ (CuKα) = 1.54184 Å. [b] λ (MoKα) = 0.71073 Å.

Figure Captions

Figure 1. Molecular structures of (a) the dimer $[Li\{S(H)C(PPh_2S)_2\}]_2$ $[Li_2\cdot(\mathbf{3})_2]$, and (b) the homoleptic complex $[Zn\{S(H)C(PPh_2S)_2\}_2]$ (**4**). Hydrogen atoms of the phenyl groups have been omitted for clarity. Weak Zn−S(P) contacts are indicated with dashed lines. Symmetry operations: A 2-x, 1-y, -z; B 1-x, 2-y, -z.

Figure 2. Molecular structures of (a) the octahedral isomer (**5a**) and (b) the square-planar isomer (**5b**) of $[Ni\{S(H)C(PPh_2S)_2\}_2]$. Hydrogen atoms of the phenyl groups and solvent molecules have been omitted for clarity. Symmetry operations: A -x, -y, 2-z; B -x, -y, 1-z.

Figure 3. Variable temperature $^{31}P\{^1H\}$ NMR spectra of $[Ni\{S(H)C(PPh_2S)_2\}_2]$ (**5**).

Figure 4. ^{31}P CP/MAS NMR spectrum of $[Ni\{S(H)C(PPh_2S)_2\}_2]$ (**5b**) at room temperature; resonances 1 and 2 are attributed to the isotropic signals of compound **5b**, resonance 3 is assigned to the isotropic signal of $[H_2C(PPh_2S)_2]$, and ssb1-ssb3 indicate the corresponding spinning sidebands.

Figure 5. Optimized geometries of singlet state square-planar (**5b**) and octahedral (**5b'**) isomers (left-hand side), and triplet state octahedral (**5a**) and square-planar (**5c**) isomers (right-hand side).

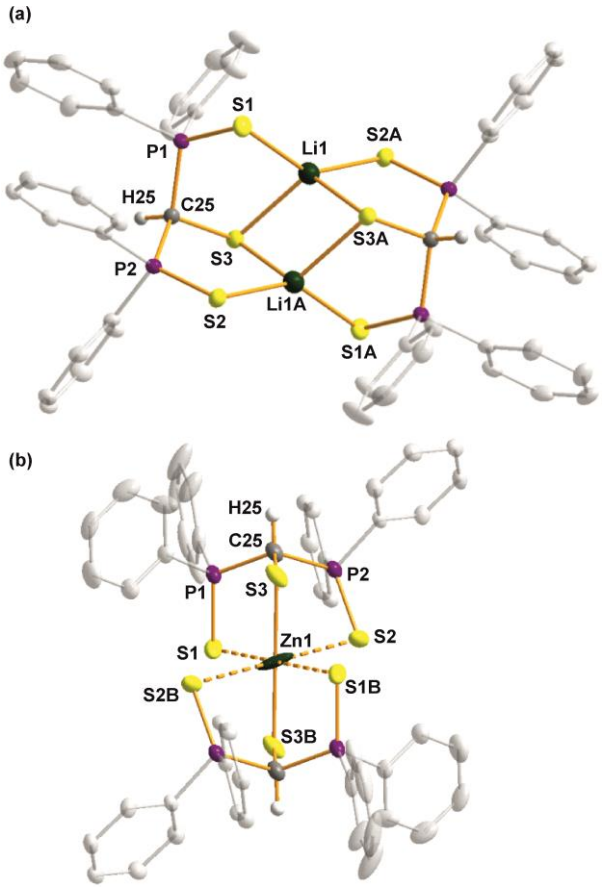
(a)
S1
P1
Li1
S2A
H25
C25
S3A
S3
P2
Li1A
S2
S1A
(b)
H25
C25
P2
P1
S3
S1
Zn1
S2
S2B
S1B
S3B

Figure 1.

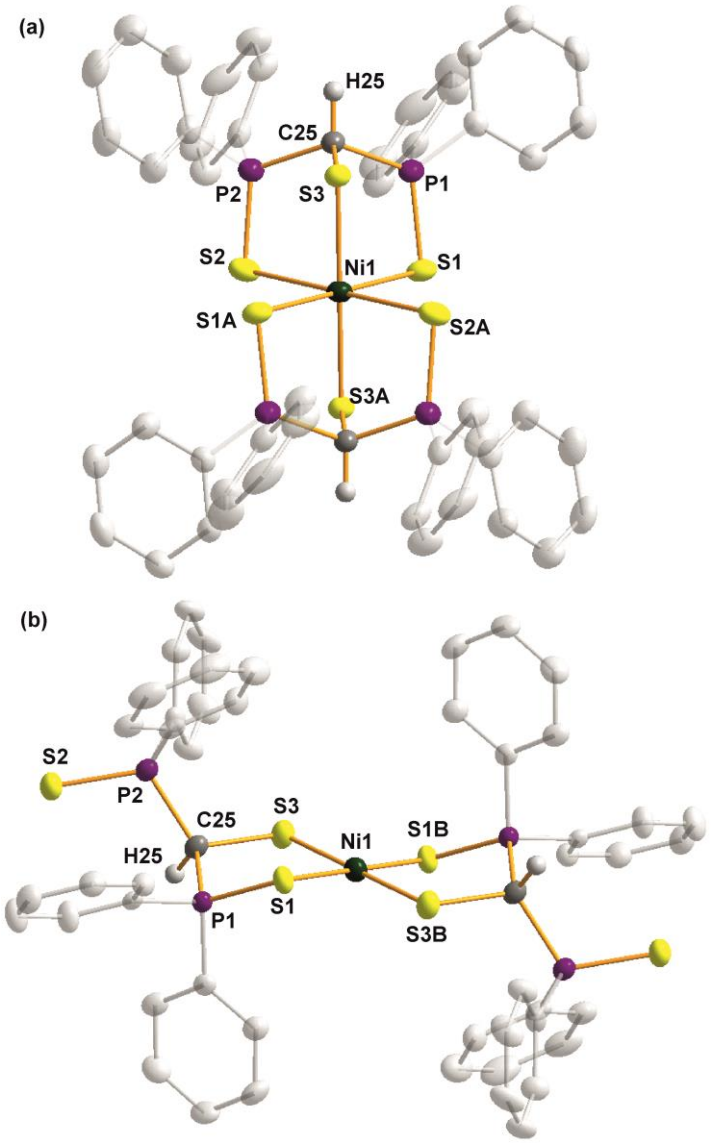
(a)
H25
C25
P2
S3
P1
S2
Ni1
S1
S1A
S2A
S3A
(b)
S2
P2
C25
S3
Ni1
S1B
H25
P1
S1
S3B

Figure 2.

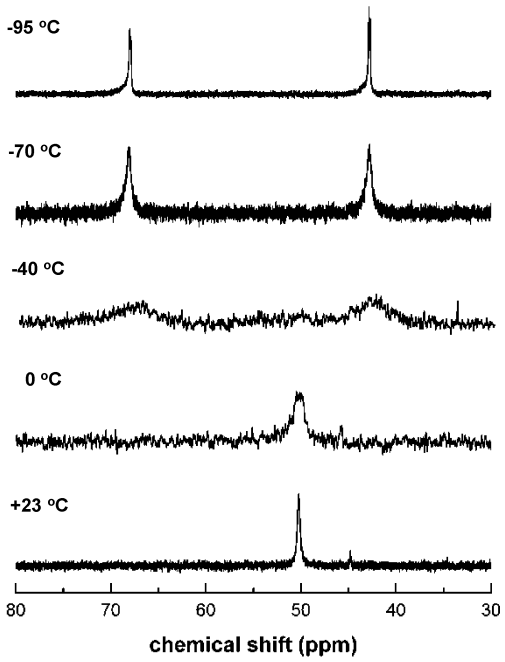

Figure 3.

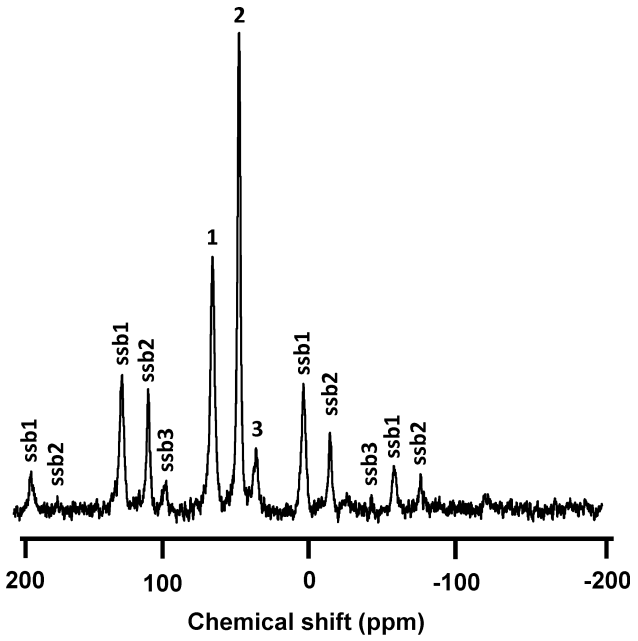
2
1
3
ssb1
ssb2
ssb3
ssb1
ssb2
ssb3
ssb1
ssb2
ssb1
ssb2
200
100
0
-100
-200
Chemical shift (ppm)

Figure 4.

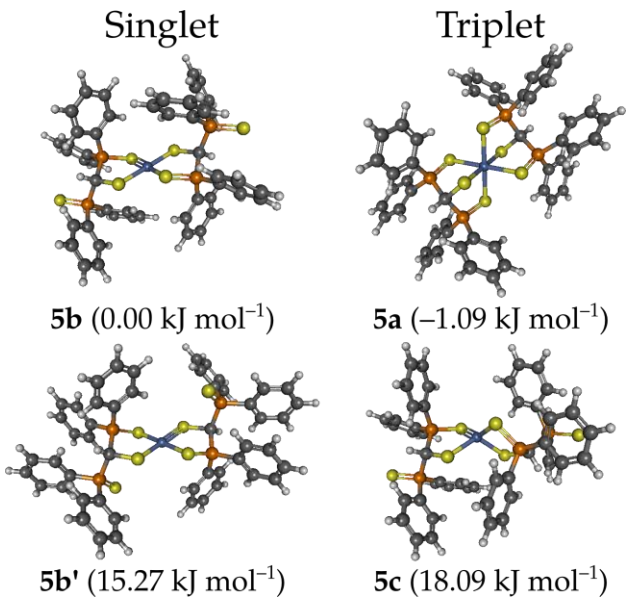
Singlet
Triplet
5b (0.00 kJ mol–1)
5a (–1.09 kJ mol–1)
5b' (15.27 kJ mol–1)
5c (18.09 kJ mol–1)

Figure 5.